PAPER

Optimizing the temporal and spatial resolutions and light throughput of Fresnel incoherent correlation holography in the framework of coded aperture imaging

IOP Publishing Journal of Optics
J. Opt. **26** (2024) 035605 (11pp) https://doi.org/10.1088/2040-8986/ad2620

Optimizing the temporal and spatial resolutions and light throughput of Fresnel incoherent correlation holography in the framework of coded aperture imaging

Francis Gracy Arockiaraj[1,2,5], Agnes Pristy Ignatius Xavier[1,2,5], Shivasubramanian Gopinath[1,5], Aravind Simon John Francis Rajeswary[1], Saulius Juodkazis[3,4] and Vijayakumar Anand[1,3,*]

[1] Institute of Physics, University of Tartu, W. Ostwaldi 1, 50411 Tartu, Estonia
[2] School of Electrical and Computer Engineering, Ben Gurion University of the Negev, PO Box 653, Beer-Sheva 8410501, Israel
[3] Optical Sciences Center and ARC Training Centre in Surface Engineering for Advanced Materials (SEAM), School of Science, Computing and Engineering Technologies, Swinburne University of Technology, Hawthorn, Melbourne VIC 3122, Australia
[4] Tokyo Tech World Research Hub Initiative (WRHI), School of Materials and Chemical Technology, Tokyo Institute of Technology, 2-12-1, Ookayama, Meguro-ku, Tokyo 152-8550, Japan

E-mail: vanand@swin.edu.au

Received 4 October 2023, revised 29 November 2023
Accepted for publication 5 February 2024
Published 14 February 2024

Abstract

Fresnel incoherent correlation holography (FINCH) is a well-established digital holography technique for 3D imaging of objects illuminated by spatially incoherent light. FINCH has a higher lateral resolution of 1.5 times that of direct imaging systems with the same numerical aperture. However, the other imaging characteristics of FINCH, such as axial resolution, temporal resolution, light throughput, and signal-to-noise ratio (SNR), are lower than those of direct imaging systems. Different techniques were developed by researchers around the world to improve the imaging characteristics of FINCH while retaining the inherent higher lateral resolution of FINCH. However, most of the solutions developed to improve FINCH presented additional challenges. In this study, we optimized FINCH in the framework of coded aperture imaging. Two recently developed computational methods, such as transport of amplitude into phase based on the Gerchberg Saxton algorithm and Lucy–Richardson–Rosen algorithm, were applied to improve light throughput and image reconstruction, respectively. The above implementation improved the axial resolution, temporal resolution, and SNR of FINCH and moved them closer to those of direct imaging while retaining the high lateral resolution. A point spread function (PSF) engineering technique has been implemented to prevent the low lateral resolution problem associated with the PSF recorded using pinholes with a large diameter. We believe that the above developments are beyond the state-of-the-art of existing FINCH-scopes.

[5] These authors contributed equally to this work.
[*] Author to whom any correspondence should be addressed.

Keywords: incoherent digital holography, Fresnel incoherent correlation holography, Lucy–Richardson–Rosen algorithm, 3D imaging, coded aperture imaging, Gerchberg–Saxton algorithm

1. Introduction

Fresnel incoherent correlation holography (FINCH) is a well-known incoherent digital holography technique [1, 2]. FINCH was developed by Rosen and Brooker in 2007 for 3D imaging of incoherently illuminated objects. In FINCH, light from an object point is split into two and differently modulated using two diffractive lenses with different focal lengths and interfered to form the self-interference hologram. In the first version of FINCH, phase masks formed by random multiplexing of two diffractive lens phase masks with three relative phase shifts $\theta = 0$, $2\pi/3$ and $4\pi/3$ were displayed on a spatial light modulator (SLM) one after the other, and the resulting three holograms are recorded. The recorded holograms are combined to create a complex hologram, which is numerically backpropagated in the computer to reconstruct the object information at any plane of interest without twin image and bias terms. At the time of the invention of FINCH in 2007, there was no existing incoherent 3D imaging technique that was as robust and simple as FINCH. In a way, FINCH created a new direction for modern day incoherent digital holography technologies. FINCH gained much attention after its demonstration on a fluorescence microscope [2] resulting in one of the highly researched topics and patented technologies in the area of incoherent imaging.

During subsequent research on FINCH, again by the same team of Rosen and Brooker, the super-resolution capability of FINCH was revealed [3]. FINCH has a resolving power that is 2 times and 1.5 times that of coherent and incoherent imaging systems with the same numerical aperture (NA), respectively. The resolution enhancement in FINCH is unlike any other resolution enhancement methods, such as structured illumination (SI) [4]. In FINCH, the resolution enhancement is obtained by shaping the modulation transfer function (MTF) within the spatial frequency boundaries imposed by the NA, whereas in the SI approach, the bandwidth of MTF is changed. In a direct incoherent imaging system, the MTF has a high response for low spatial frequencies and a low response for high spatial frequencies. In FINCH, at the optimal operating conditions, the MTF has a uniform response. With SI, when the MTF is expanded, the fundamental response structure of the MTF of direct imaging is carried on, preventing the realization of the full potential of SI. Therefore, FINCH can be considered a more fundamental imaging system with the optimal MTF that can be used as a platform for applying other super-resolution technologies such as SI [5]. The unusual MTF of FINCH results in surprising imaging characteristics. The magnification of spacing between two points is twice as much as the magnification of a point when imaging using FINCH with an optimal optical configuration. Besides, the axial resolution of FINCH is lower than that of an incoherent imaging system with the same NA. When the super-resolution capability of FINCH was demonstrated, the optical configuration of FINCH was also upgraded from spatial multiplexing with a random mask to polarization multiplexing method, which improved the signal-to-noise ratio (SNR) significantly. The evolution of FINCH is presented in detail in [3, 6].

Starting from the version of FINCH demonstrated in [3], FINCH evolved rapidly over the past decade with contributions made by leading researchers around the world [6–8]. Before describing the contributions of different groups in FINCH, the state-of-the-art FINCH in 2012 is presented. The reported version of FINCH in [3] used a polarization multiplexing approach and recorded three phase-shifted holograms with three camera shots. Spatial resolutions—lateral and axial resolutions, define how well the information is discriminated in space along the transverse and longitudinal directions, respectively. Similarly, temporal or time resolution defines how well the information is discriminated in time. When recording static scenes, temporal resolution is not critical. However, when recording dynamic scenes, temporal resolution is critical. In this study, temporal resolution is defined as the inverse of the number of camera shots needed to capture a scene. A higher number of camera shots means lower temporal resolution and vice versa. This version [3], when compared to direct incoherent imaging systems with the same NA, exhibited a superior lateral resolution but an inferior axial resolution and an inferior temporal resolution of one-third. The light throughput in FINCH is about 25% of that of other incoherent imaging systems. With implementation, FINCH required an active device like an SLM and numerous optical elements such as lenses and polarizers. Many developments were made in FINCH to reduce one or many of the above disadvantages, out of which some key contributions are described next.

Several groups attempted to improve the temporal resolution of FINCH to match that of direct incoherent imaging systems. Spatial multiplexing methods were reported by Nobukawa and Nomura [9, 10], polarization multiplexing method using a 4-pol image sensor where every pixel consists of a 2×2 array of polarizers at $0°$, $45°$, $90°$, and $135°$ was reported by Tahara *et al* [11]. The above methods improved the temporal resolution of FINCH at the expense of field-of-view [9, 10] and SNR [11]. Passive optical elements such as geometric lens [12] and metasurfaces [13] were manufactured to make FINCH compact and lightweight by Liu and Huang, respectively. Different recording and reconstruction methods were reported by Tahara *et al* [14] and Anand *et al* [15]. While the approach of Tahara *et al* [14] required at least two camera shots for FINCH, the approach of Anand *et al* [15]

demonstrated a single camera shot FINCH with a one-time recorded point spread function (PSF) and non-linear reconstruction (NLR) method [16]. The low axial resolution of FINCH was addressed by building a confocal FINCH with a scanning pinhole [17]. FINCH concept was adapted for other applications such as localization microscopy [18, 19], light sheet microscopy [20], and advanced manufacturing [21].

FINCH in different configurations has a different set of challenges. In the widely used configuration of imaging, FINCH has one-half of the temporal resolution [13], one-fourth of light throughput, and lower axial resolution than other incoherent imaging systems. The implementation of FINCH requires either an SLM or other liquid crystal elements [22]. In all the above studies, every solution came with a problem except for [14]. The study [15] was peculiar as FINCH was implemented as a coded aperture imaging (CAI) method [23]. This is the only study where the axial resolution of FINCH was improved unexpectedly. A follow-up study of FINCH as CAI confirmed the improvement in the axial resolution of FINCH [24]. One drawback of [15] was that the random multiplexing method used for creating the phase masks and the NLR method resulted in a low SNR. Recently, advancements have been made on the above two fronts. A novel computational algorithm called transport of amplitude into phase based on Gerchberg Saxton algorithm (TAP-GSA) for spatially multiplexing two phase masks with minimum random noises and a high SNR reaching the limit of direct incoherent imaging was developed [25]. An advanced computational reconstruction method called Lucy–Richardson–Rosen algorithm (LR^2A) was developed as a better alternative to NLR and implemented in many studies for 3D imaging [26–28]. A preliminary study of FINCH using TAP-GSA and LR^2A was carried out, which demonstrated a superior performance of FINCH [29]. One recent study combined FINCH with another holography technique called coded aperture correlation holography (COACH) [30] to obtain the axial resolution of COACH and lateral resolution of FINCH [31]. This new technique is called coded aperture with FINCH intensity responses (CAFIR). However, CAFIR required three camera shots. A most recent study from our research group on self-wavefront incoherent transverse splitting holography (SWITSH), a derivative of FINCH, showed promising results of a single shot with LR^2A.

In this study, we attempt to optimize FINCH on all the aspects of imaging using TAP-GSA, LR^2A, and PSF engineering with all known advantages and devoid of the inherent disadvantages of FINCH. The optimized FINCH, has the same temporal resolution, axial resolution, same light throughput, and SNR as a direct incoherent imaging system and retains the advantages such as the superior lateral resolution and 3D imaging capability. The proposed FINCH with the above collection of methods can be implemented with a passive diffractive element that does not require a vibration isolation system and additional optical components. The PSF engineering approach allows to shift the lateral resolution limit from the size of the pinhole to that defined by the NA of the imaging system. The rest of the manuscript is organized as follows. The methodology is presented in the second section. The simulation studies of 2D and 3D imaging are presented in the third section. In the fourth section, experimental results are presented. The conclusion and future perspectives are presented in the final section.

2. Materials and methods

The computational optical configuration of FINCH implemented as a CAI system is shown in figure 1. The imaging process consists of three major steps: mask design, optical recording, and computational reconstruction. In the first step, the two phase-only diffractive lens masks are spatially multiplexed to form a single phase-only mask using TAP-GSA [25]. The designed mask is either manufactured using lithography techniques or displayed on an SLM to record the point spread hologram (I_{PSH}) in the first step and an object hologram (I_{OH}) in the next step under identical recording conditions [24]. In the third and final step, the recorded holograms are reconstructed using LR^2A with suitable conditions to obtain optimal reconstruction results [26]. Assuming that the distances are large, Fresnel approximation-based equations are used for analyzing the system. A point object emitting light with an amplitude of $\sqrt{I_o}$ is considered. The point object is located at a distance of z_s from a refractive lens L as shown in figure 1. To achieve the optimal FINCH condition of super-resolution, it is necessary to have the same beam diameter for the two beams at the sensor plane located at a distance of z_h from the SLM. The elements L and SLM are assumed to be in tandem to simplify the analysis. To achieve the optimal FINCH condition, when the object distance z_s equals the focal length f of the refractive lens L, the focal length of the two diffractive lenses need to be $z_h/2$ and ∞ respectively. Only for the plane $z_s = f$, FINCH exhibits an optimal resolution and has a lower resolution in other planes. The phase function of the two lenses are $\exp\left(-ikr^2/z_h\right)$ and 1, where $r = \sqrt{x^2+y^2}$ and $k = 2\pi/\lambda$ and λ is the wavelength. Using TAP-GSA, the two lenses are combined to form a phase-only diffractive element given as $\exp\left[ikP(x,y)\right] = 1 + \exp\left(-ikr^2/z_h\right)$, where $P(x,y)$ is the optical path length variation.

The complex amplitude from the point object reaching the lens L is $C_1\sqrt{I_o}Q(1/z_s)$, where C_1 is a complex constant, Q is a quadratic phase function given as $Q(a) = \exp\left(ikar^2/2\right)$. The complex amplitude after the lens L is $C_2\sqrt{I_o}Q(1/z_s)Q(-1/f)$, and the complex amplitude after the SLM is $C_3\sqrt{I_o}Q(1/z_s)Q(-1/f)\exp\left[ikP(x,y)\right]$, where C_2 and C_3 are complex constants. The PSH recorded at the sensor plane is given as

$$I_{PSH} = \left|C_3\sqrt{I_o}Q(1/z_s)Q(-1/f)\exp\left[ikP(x,y)\right] \otimes Q(1/z_h)\right|^2, \quad (1)$$

where '$\otimes$' is a 2D convolutional operator. If O is a multi-point object, then the object hologram (I_{OH}) can be given as $I_{OH} = O \otimes I_{PSH}$. In conventional FINCH, i.e. as a digital holography system, at least three camera shots with three different phase shifts are recorded and combined to form a complex hologram. This complex hologram, when numerically back propagated, reconstructs the object information without

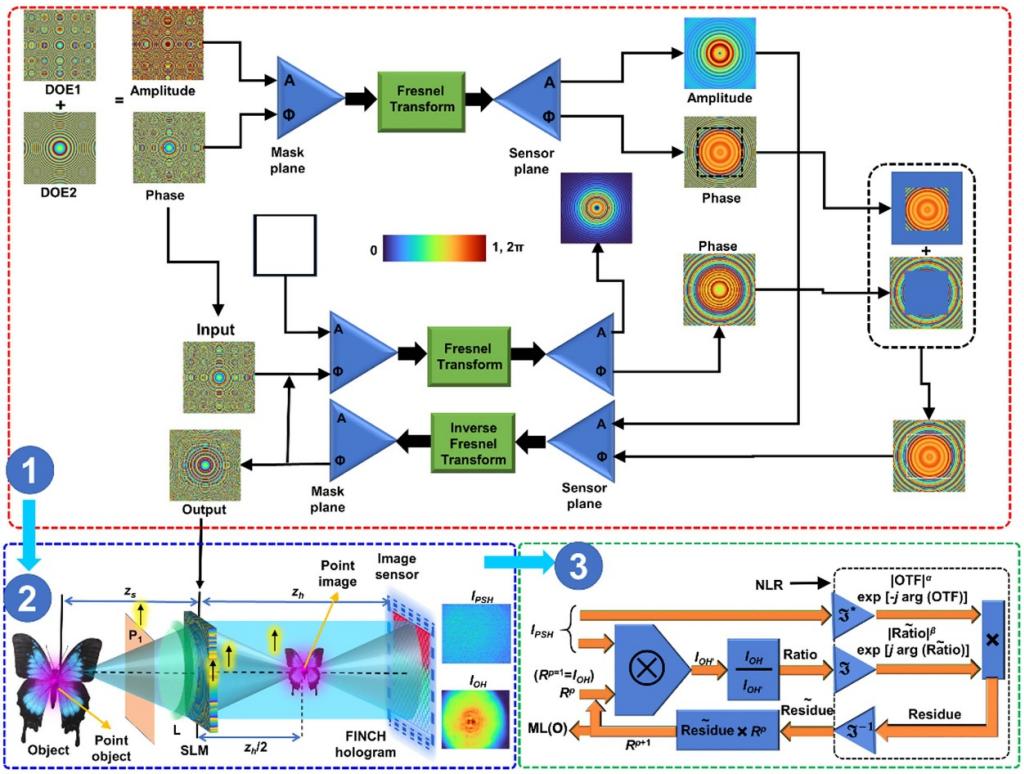

Figure 1. Computational optical configuration of FINCH as a CAI system. The technique consists of three major steps: computational mask design using TAP-GSA, optical FINCH experiment and recording of PSH and OH and computational reconstruction using LR^{2}A. OTF—optical transfer function; p—number of iterations; $\otimes$—2D convolutional operator; $\Im^*$—refers to complex conjugate following a Fourier transform; $\Im^{-1}$- Inverse Fourier transform; R^p is the pth solution and p is an integer, when $p=1$, $R^p = I_{\mathrm{OH}}$; ML—maximum likelihood; α and β are varied from -1 to 1. The LR^{2}A is given by the following mathematical operator '$\circledcirc$'.

the twin image and bias terms. In FINCH, the super resolution is not originated from the phase-shifting but from the recording configuration. So, the super resolution features are present in every FINCH hologram recorded under optimal conditions. Now applying the concepts of CAI, the image of the object can be reconstructed by a correlation. The reconstructed image (I_{R}) is given as $I_{\mathrm{R}} = I_{\mathrm{OH}} * I_{\mathrm{PSH}}$, where '$*$' is a 2D correlation operator. Substituting for I_{OH} in the above equation, we obtain $I_{\mathrm{R}} = O \otimes I_{\mathrm{PSH}} * I_{\mathrm{PSH}}$. If $I_{\mathrm{PSH}} * I_{\mathrm{PSH}}$ is a Delta-like function, then the expression is simplified further as $I_{\mathrm{R}} = O \otimes \delta$. Instead of correlation, in this study LR^{2}A which has been proved to generate sharpest Delta-like functions for deterministic optical fields [28]. The I_{R} with LR^{2}A is given as $I_{\mathrm{R}} = I_{\mathrm{OH}} \circledcirc I_{\mathrm{PSH}}$, where '$\circledcirc$' represents the LR^{2}A operator with optimal values of α, β, and p. While LR^{2}A is already described in [26–28], it is briefly summarized here. The LR^{2}A improves the estimation of 'O' iteratively, using the relation between I_{PSH}, O, and I_{OH}, starting from an initial guessed 'O'. The initial guessed solution for 'O' is usually I_{OH} and the relation $I_{\mathrm{OH}}{}' = O_{\mathrm{Guess}} \otimes I_{\mathrm{PSH}}$ is validated, and the ratio between the recorded I_{OH} and the estimated I_{OH}' is calculated. This ratio is correlated with I_{PSH} using NLR and the discrepancy in the previous solution is obtained indicated as *Residue* in part—3 of figure 1. This is multiplied to the previous solution of 'O' and this entire process is iterated until the estimated solution converges as close as possible to 'O'. The use of NLR estimates the discrepancy in O in every iteration with a high SNR contributing to an accelerated and improved estimation of O.

To summarize, there are three innovations applied in FINCH simultaneously: TAP-GSA, CAI framework with LR^{2}A, and PSF engineering. While the method is analytically studied above, the key equations corresponding to the above methods are presented here. Using TAP-GSA, the following approximation has been achieved, $\exp[ikP(x,y)] \sim 1 + \exp\left(-ikr^2/z_{\mathrm{h}}\right)$, where a pure phase function is generated from a complex function by transporting the magnitude of the complex function to the phase. Using the CAI framework and LR^{2}A, single shot reconstruction with a high SNR is achieved using $I_{\mathrm{R}} = I_{\mathrm{OH}} \circledcirc I_{\mathrm{PSH}}$. Using PSF engineering, the ideal I_{PSH} is synthesized from recorded approximate I_{PSH} using $I_{\mathrm{PSH(ideal)}} = O \circledcirc I_{\mathrm{PSH(recorded)}}$.

In the previous studies [15, 24], the resolution limit of FINCH was affected by the size of the pinhole. In this study, the I_{PSH} is engineered as follows. A I_{PSH} is recorded for a pinhole and used as I_{OH} along with the direct imaging result O of the pinhole to estimate the ideal I_{PSH}. The ideal I_{PSH} is given as$I_{\mathrm{PSH}} = I_{\mathrm{OH}} \circledcirc I_{\mathrm{D}}$, where I_{D} is the direct image of the pinhole. The aberration theory and related corrections are applied mostly with direct imaging concepts and not with holography techniques. The main reason for not

needing aberration concepts and corrections in many holography systems is that the phase shifting procedure, besides removing the twin image and bias terms also removes the aberrations that are common in the recorded holograms. This can be understood from the reconstruction mechanism used for conventional FINCH. The FINCH holograms recorded are not with ideal optical systems but reconstructed numerically with an ideal quadratic phase function. This is possible as the phase shifting procedure removes the aberrations present in the FINCH recording system. When implementing FINCH in the framework of CAI, the aberration function is included in the recorded I_{PSH}. During reconstruction by cross-correlation or LR^{2}A, the image of the object is reconstructed without the aberration. Therefore, it will be possible to use a synthetic ideal I_{PSH} generated in the computer to reconstruct the I_{OH} if the system is devoid of aberrations. It must be noted that this is not a special condition but the condition of most direct imaging systems. By constructing a FINCH recording setup that has minimum aberrations will enable the use of ideal synthetic I_{PSH} for reconstructing FINCH holograms in the framework of CAI. The other CAI techniques, such as CAFIR [31] and SWITSH [32] require changing the original optical configuration of FINCH.

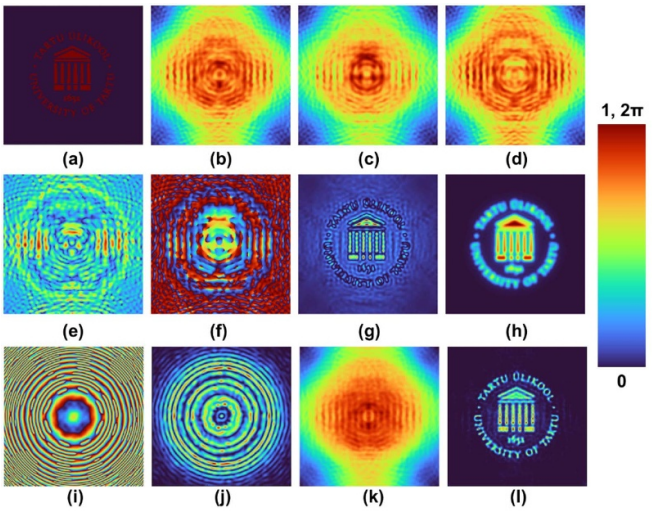

Figure 2. Simulation results of conventional FINCH. (a) Test object. FINCH holograms simulated for phase shifts $\theta =$ (b) 0, (c) $2\pi/3$ and (d) $4\pi/3$. (e) The magnitude and (f) phase of the complex hologram H_{C}. (g) Reconstruction result. (h) Direct imaging result. (i) Phase image of the mask designed using TAP-GSA with 100% DoF. Images of (j) I_{PSH}, (k) I_{OH} and (l) I_R.

3. Simulation studies

The simulation study of FINCH in the framework of CAI was carried out using MATLAB. A matrix size of 500×500 pixels was used with a pixel size $\Delta = 10$ μm and wavelength $\lambda = 650$ nm. The object distance $z_{\mathrm{s}} = 50$ cm, recording distance $z_{\mathrm{h}} = 1$ m, and the focal lengths of diffractive lenses are 25 cm and 50 cm. The logo of University of Tartu was used as a test object for the simulation studies, as shown in figure 2(a). For conventional FINCH, three holograms I_{OH1}, I_{OH2} and I_{OH3} are simulated with phase shifts $\theta = 0$, $2\pi/3$ and $4\pi/3$ respectively, and combined as $H_{\mathrm{C}} = I_{\mathrm{OH1}}\left(\exp\left[-i4\pi/3\right] - \exp\left[-i2\pi/3\right]\right) + I_{\mathrm{OH2}}\left(1 - \exp\left[-i4\pi/3\right]\right) + I_{\mathrm{OH3}}\left(\exp\left[-i2\pi/3\right] - 1\right)$. The complex hologram H_{C} is propagated numerically to the plane of the object by $I_{\mathrm{R}} = H_{\mathrm{C}} \otimes Q\left(1/z_{\mathrm{R}}\right)$, where z_{R} is the reconstruction distance which is 50 cm in this case. The images of I_{OH1}, I_{OH2} and I_{OH3} are shown in figures 2(b)–(d) respectively. The magnitude and phase of H_{C} are shown in figures 2(e) and (f) respectively. The reconstructed image I_{R} is shown in figure 2(g). The direct imaging result is shown in figure 2(h). Comparing figures 2(g) and (h), an improvement in lateral resolution can be observed for FINCH.

When FINCH is implemented as CAI, there are only two holograms needed: I_{PSH} and I_{OH}. The image is reconstructed by processing the above holograms using LR^{2}A. But the phase mask is designed using TAP-GSA. The image of the phase mask designed with >90% degrees of freedom (DoF) is shown in figure 2(i). The I_{PSH} and I_{OH} are shown in figures 2(j) and (k) respectively. The reconstructed image using LR^{2}A is shown in figure 2(l). Comparing figure 2(l) with figures 2(g) and (h), an improvement in lateral resolution with respect to 2(h) and a higher SNR compared to 2(g) are seen. The structural similarity index (SSIM) values for FINCH as CAI, direct imaging, and FINCH with three shots are 0.7038, 0.6529, and 0.0417, respectively. The simulation study shows a higher SNR quantified by SSIM in FINCH as CAI compared to both direct imaging and conventional FINCH. However, the lateral resolutions of figures 2(g) and (l) are the same.

The axial characteristics are investigated next. In general, the axial range and increment for understanding the axial characteristics are decided based on various factors such as object size, nature of the optical field, and computational resource. The object size dictates the axial range, and the nature of optical field dictates the increment. In [6, 32], CAI was realized using a scattering mask, and so it was sufficient to simulate or record the I_{PSH}s at the two axial boundaries of z_{s} and the intermediate distributions can be synthesized using a scaling factor. However, in FINCH, the above is not possible as the self-interference distributions at different planes cannot be synthesized using a scaling factor. Therefore, in FINCH, it is necessary to record I_{PSH}s at multiple axial locations. In this simulation study, the axial range and increment were decided based on the computational resource (1.8 GHz processor, 16 GB RAM, and 64-bit operating system) and the optical field such that a smooth axial correlation curve could be obtained. A point object is considered, which is shifted from $z_{\mathrm{s}} = 30$ cm to 70 cm in steps of 4 mm, and the FINCH hologram is simulated and reconstructed with the reconstructing function corresponding to $z_{\mathrm{s}} = 25$ cm. In the case of conventional FINCH, the reconstruction distance was maintained the same at $z_{\mathrm{R}} = 25$ cm, and in the case of FINCH as CAI, the I_{PSH} corresponding to $z_{\mathrm{s}} = 25$ cm is used. The normalized intensity value of the reconstructed point object at the optical

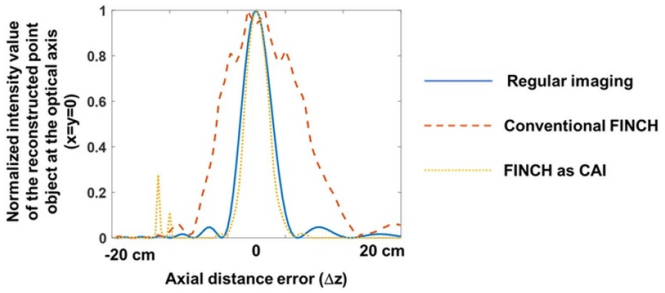

Figure 3. Plots of axial correlation curves for direct imaging, conventional FINCH and FINCH as CAI.

axis ($x = y = 0$) is plotted for direct imaging, conventional FINCH, and FINCH as CAI, as shown in figure 3. It can be seen from the plots that FINCH, when implemented as CAI, has a higher axial resolution than conventional FINCH and the same axial resolution as a direct imaging system. So unlike CAFIR, where the axial resolution of COACH and lateral resolution of FINCH was obtained, in the proposed approach, FINCH as CAI, the above high axial and lateral resolution has been achieved without any modification to the phase mask.

The primary lateral resolution limit in CAI methods is imposed by the NA of the system given as $\sim\lambda$/NA. As long as the diameter d of the pinhole used for recording I_{PSH} is smaller than λ/NA, there is no secondary resolution limit. When $d > \lambda$/NA, the pinhole samples the object with a low resolution. In a typical experiment, the lateral resolution limit imposed by NA is 1–10 μm, which demands a high photon budget to bring the intensity distribution within the dynamic range of the camera. Even if the above is achieved, the noise level in the detector is same as the signal level, resulting in a low SNR. Therefore, in many CAI techniques [26–28], some resolution was often sacrificed to achieve a high SNR. In FINCH as CAI, we investigate the possibilities of synthesizing an ideal I_{PSH} from I_{PSH} recorded for pinhole with a large d. A two-step reconstruction procedure is implemented: in the first step, the ideal I_{PSH} is synthesized from recorded I_{PSH} and direct image of the pinhole, and the ideal I_{PSH} is used to reconstruct the object's image from I_{OH}. In the configuration used for simulation, the diffraction limited spot size is 160 μm and, so d was set as 160 μm. An USAF 1951 object was used as the test object. The image of the test object, I_{PSH}, I_{OH}, and reconstructed result from LR^{2}A are shown in figures 4(a)–(d) respectively. The images of the I_{PSH} for $d = 400$ μm and the corresponding reconstruction result are shown in figures 4(e) and (f), respectively. The images of the engineered ideal I_{PSH}s obtained from figure 4(e) is shown in figure 4(g). Comparing figures 4(b), (e) and (g), a better match is seen between figures 4(b) and (g) than between figures 4(b) and (e). The reconstruction results of LR^{2}A using the ideal I_{PSH} shown in figure 4(g) is shown in figure 4(h). As it is seen, the image recovered from the ideal I_{PSH} has a better match with the reference image compared to the image recovered from the I_{PSH} obtained using a large pinhole. There are some loss of information and distortion but the higher resolution inherent in FINCH is preserved.

4. Experiments

The photograph of the FINCH experimental setup is shown in figure 5. The FINCH setup consists of the following components: high-power LED (Thorlabs, 940 mW, $\lambda = 660$ nm and $\Delta\lambda = 20$ nm), iris, diffuser (Thorlabs Ø1″ Ground Glass Diffuser-220 GRIT), polarizer, refractive lenses, object/pinhole, beam splitter, SLM (Thorlabs Exulus HD2, 1920 × 1200 pixels, pixel size = 8 μm) and an image sensor (Zelux CS165MU/M 1.6 MP monochrome CMOS camera, 1440 × 1080 pixels with pixel size ∼3.5 μm). The light emitted from the high-power LED entered the set up through the iris, which was used to control the diameter of the incoming light. Next, a diffuser was used to remove the grating lines of the LED from the incoming light. A refractive lens (L1) with a focal length of 10 cm was used to collimate the light from the diffuser. A polarizer was used to polarize the light along the active axis of the SLM. The light from the polarizer entered another refractive lens (L2) with a focal length 5 cm, which critically illuminated the object. The light from the object was collimated using another refractive lens (L3) with a focal length 5 cm, and it was placed at a distance of $z_{\mathrm{s}} = 5$ cm from the object. The collimated light entered the beam splitter and reached the SLM. The phase shifted masks synthesized using TAP-GSA algorithm were displayed on the SLM, and the FINCH holograms were recorded by the image sensor placed at a distance of $z_{\mathrm{h}} = 21$ cm from the SLM. The objects digit '1' and '3', were used from Group—5 from R1DS1N—Negative 1951 USAF Test Target, Ø1" for demonstration. The I_{PSH} was recorded using a 25 μm pinhole.

Multiple experiments were carried out in the set up. In the first experiment, single plane imaging was carried out to compare the SNR and root mean squared error (RMSE) between conventional FINCH with three camera shots and FINCH based on CAI. The digit '1' from Group—5 was used for this study. The TAP-GSA was run with a DoF of 98%. The images of the phase masks designed using TAP-GSA for $\theta = 0$, $2\pi/3$, and $4\pi/3$ are shown in figures 6(a)–(c), respectively. The recorded FINCH holograms I_{OH}s for the object digit '1' for $\theta = 0$, $2\pi/3$ and $4\pi/3$ are shown in figures 6(d)–(f) respectively. The above three holograms were combined to form a complex hologram whose magnitude and phase are shown in figures 6(g) and (h) respectively. The reconstructed image using numerical back propagation by a distance of approximately 10 cm for conventional FINCH is shown in figure 6(i). The FINCH hologram I_{PSH}s for a pinhole with a diameter of 25 μm for $\theta = 2\pi/3$ is shown in figure 6(j). The reconstruction result by LR^{2}A for ($\alpha = 0.1$, $\beta = 1$, $p = 9$) FINCH as CAI is shown in figure 6(k). The direct imaging result is shown in figure 6(l). The SSIM and RMSE values were calculated using direct imaging result as reference and plotted in figures 6(m) and (n), respectively. The SSIM values obtained for conventional FINCH and FINCH as CAI are 0.6668 and 0.9847 respectively. The RMSE values obtained for conventional FINCH and FINCH as CAI are 0.0278 and 0.0492, respectively. By SSIM as figure of merit, FINCH as CAI using LR^{2}A has a significantly better performance in comparison to conventional FINCH. By RMSE as figure of merit, FINCH as

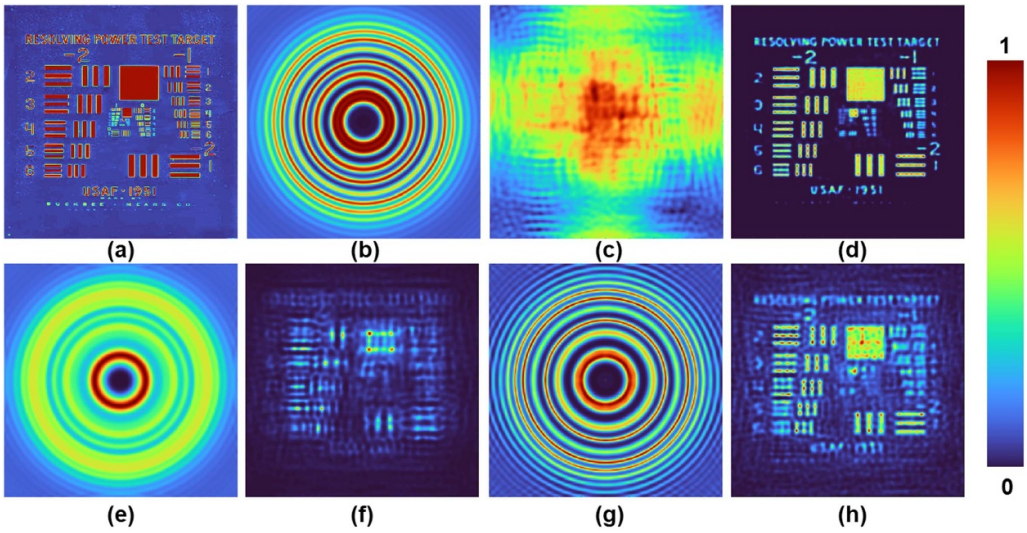

Figure 4. (a) Test object and images of (b) ideal I_{PSH}, (c) I_{OH}, (d) reconstruction. Images of (e) I_{PSH} obtained for a larger pinhole and (f) image reconstructed using (e). (g) Image of the synthesized ideal I_{PSH} and (h) its reconstruction.

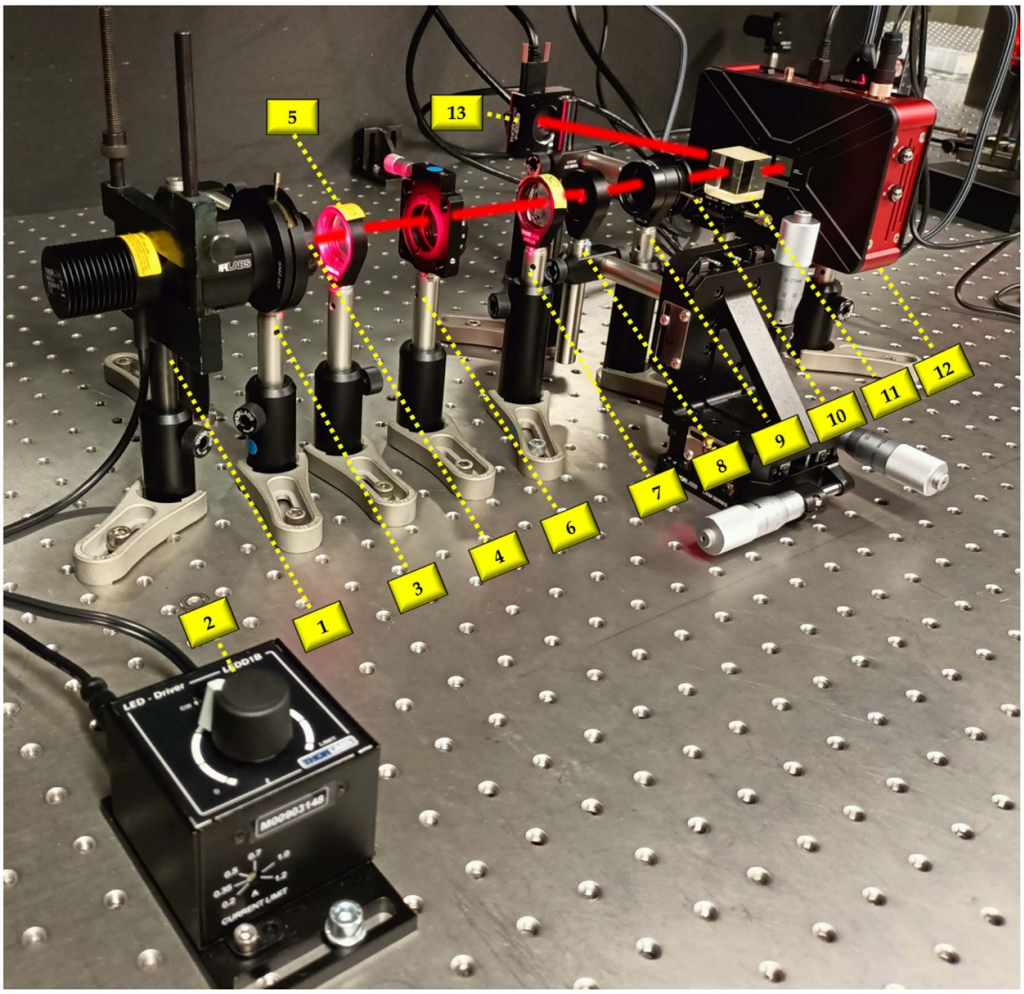

Figure 5. Photograph of FINCH experimental setup: (1) high-power LED, (2) LED power controller, (3) iris, (4) diffuser, (5) refractive lens L1, (6) polarizer, (7) refractive lens L2, (8) object/pinhole, (9) refractive lens L3, (10) iris, (11) beam splitter, (12) spatial light modulator, (13) image sensor. (The red line shows the path of the light beam).

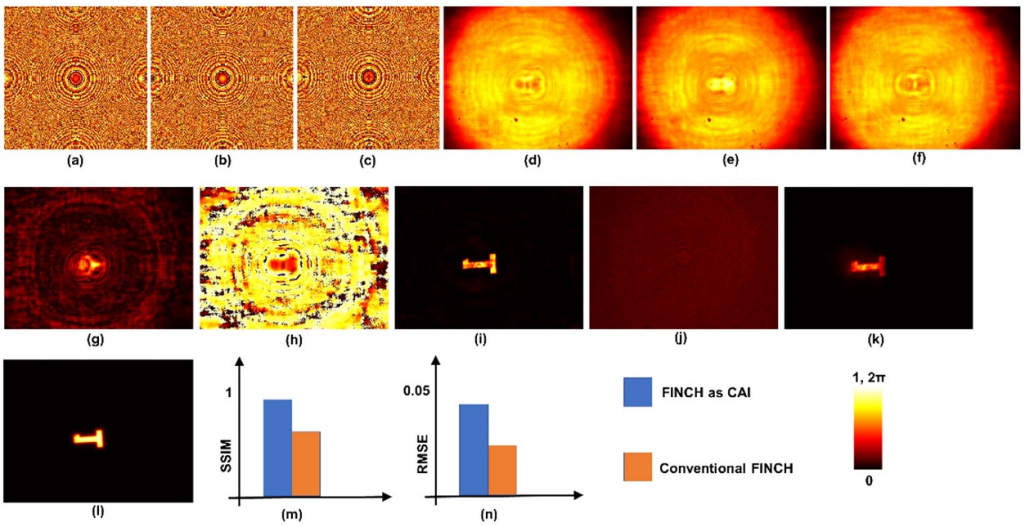

Figure 6. Images of the phase masks designed using TAP-GSA with phase shifts (a) $\theta = 0$, (b) $\theta = 2\pi/3$ and (c) $\theta = 4\pi/3$. I_{OH} recorded using phase masks with phase shifts (d) $\theta = 0$, (e) $\theta = 2\pi/3$ and (f) $\theta = 4\pi/3$. (g) Magnitude and (h) phase of the complex hologram. (i) Reconstruction result of conventional FINCH. (j) I_{PSH} recorded for $\theta = 2\pi/3$. (k) Reconstruction result of FINCH as CAI. (l) Direct imaging result. (m) Plot of SSIM for conventional FINCH and FINCH as CAI. (n) Plot of RMSE for conventional FINCH and FINCH as CAI.

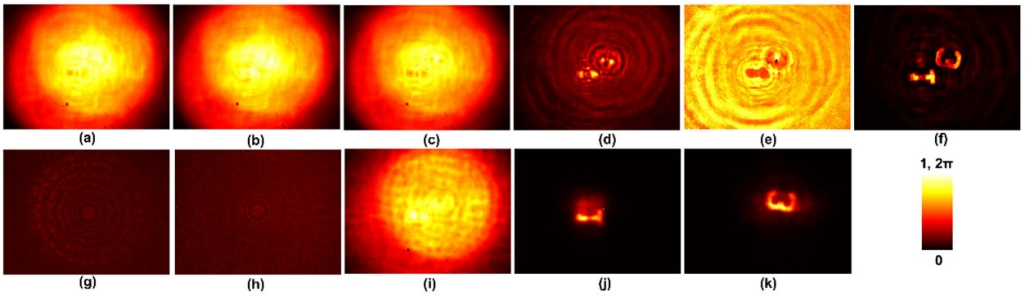

Figure 7. I_{OH} recorded using phase masks with phase shifts (a) $\theta = 0$, (b) $\theta = 2\pi/3$ and (c) $\theta = 4\pi/3$. (d) Magnitude and (e) phase of the complex hologram. (f) Reconstruction result of conventional FINCH. (g) I_{PSH} recorded for $z_{\mathrm{s}} = 5$ cm. (h) I_{PSH} recorded for $z_{\mathrm{s}} = 5.6$ cm. (i) I_{OH} for the object with two planes. (j) Reconstruction result using I_{PSH} recorded for $z_{\mathrm{s}} = 5$ cm. (k) Reconstruction result using I_{PSH} recorded for $z_{\mathrm{s}} = 5.6$ cm.

CAI has nearly the same performance as conventional FINCH. The above two comparison results indicate a better performance of the proposed method over the conventional method. The average execution time of TAP-GSA and LR^{2}A using a computer with an AMD Ryzen 5 3450U 2.10 GHz processor, 8.00 GB RAM and 64-bit operating system are approximately 3 min and 7 s respectively. During the study, it was noticed that conventional FINCH does not give an optimal result for all values of DoF, and so different masks were tried for conventional FINCH, whereas FINCH as CAI generated consistent result for different values of DoF. In the rest of the manuscript, only the optimal results of conventional FINCH were shown, but FINCH as CAI experiment was carried out with the phase mask with DoF $= 98\%$.

In the next experiment, the axial resolution of FINCH as CAI was compared with conventional FINCH by a 3D imaging experiment. Two test objects, digit '1' and digit '3', were mounted at two different distances of $z_{\mathrm{s}} = 5$ and 5.6 cm. Conventional FINCH experiment was carried out using phase masks designed with DoF of 56%. The FINCH holograms I_{OH}s were recorded and summed to obtain the holograms for the two objects. The images of the FINCH holograms I_{OH}s, magnitude and phase of the complex hologram, and the reconstructed result are shown in figures 7(a)–(f) respectively. The image of the object was reconstructed at a distance of approximately 10 cm. The images of the I_{PSH}s recorded for $z_{\mathrm{s}} = 5$ and 5.6 cm are shown in figures 7(g) and (h), respectively. The FINCH hologram I_{OH} is shown in figure 7(i). The reconstruction results using I_{PSH} for $z_{\mathrm{s}} = 5$ and 5.6 cm are shown in figures 7(j) and (k), respectively. By comparing the results of figures 7(j) and (k), an improvement in axial resolution in FINCH as CAI can be seen in comparison to conventional FINCH. The reconstruction parameters for LR^{2}A are the same as in the previous experiment.

Next, we investigate the possibility of obtaining an ideal I_{PSH} from the recorded I_{PSH} with a pinhole with $d = 50$ μm. The image of the recorded I_{PSH} is shown in figure 8(a). The ideal I_{PSH} was engineered from the recorded I_{PSH} using the

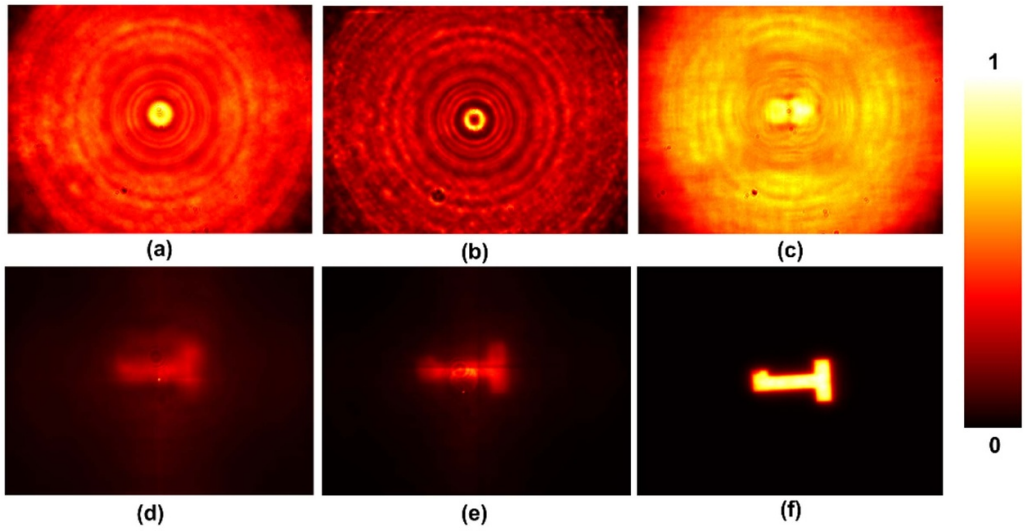

Figure 8. (a) I_{PSH} recorded using a pinhole with $d = 50$ μm. (b) Engineered ideal I_{PSH}. (c) I_{OH}. (d) Reconstruction result using recorded I_{PSH} shown in (a). (e) Reconstruction result using recorded I_{PSH} shown in (b). (f) Direct imaging result.

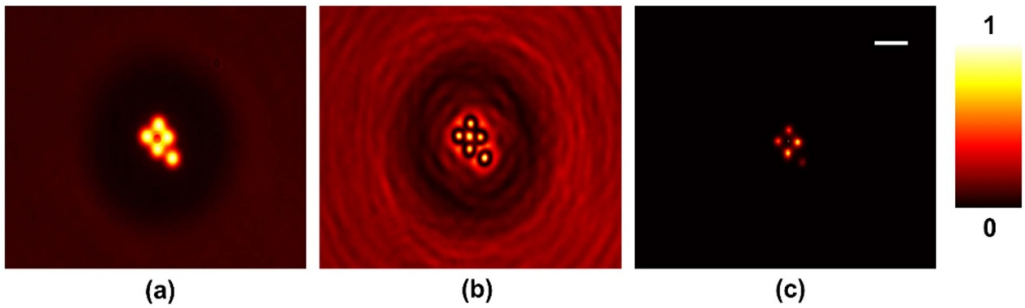

Figure 9. Reconstruction results of (a) direct imaging, (b) conventional FINCH and (c) FINCH as CAI. The line has a length of 100 μm.

direct image of the pinhole. Alternatively, it can be also be just a disc created in an empty matrix with the size of the active region of camera. The image of the synthesized ideal I_{PSH} is shown in figure 8(b). The LR^{2}A was operated with ($\alpha = 0.4$, $\beta = 1$, $p = 10$). The image of the I_{OH} is shown in figure 8(c). The reconstructed results using 8(a) and (b) are shown in figures 8(d) and (e) respectively. The LR^{2}A was operated with ($\alpha = 0.2$, $\beta = 1$, $p = 5$). The direct imaging result is shown in figure 8(f). The reconstructed result shown in figure 8(d) has a low resolution due to the large value of *d,* but the reconstructed result shown in figure 8(e) has a higher sharpness similar to the results shown in figures 6(k) and 7(j) respectively. The SSIM values of figures 8(d) and (e) are 0.9766 and 0.9782 respectively. The RMSE values of figures 8(d) and (e) are 0.0649 and 0.0634 respectively.

Finally, we verify if the presented approach using LR^{2}A and TAP-GSA preserves the high lateral resolution inherent to FINCH. To investigate this, an experiment was carried out using a pinhole with $d = 25$ μm which was shifted by the least count of the screw gauge, which is 10 μm along x and y directions, and FINCH holograms were recorded for each location and then summed. An aperture was added to the SLM to block light beyond a radius of 75 pixels. The results of direct imaging, conventional FINCH, and FINCH as CAI are shown in figures 9(a)–(c) respectively. Comparing the figures, the inherent higher resolution in FINCH is seen in both 9(b) and (c). This validates that the developed technique preserves the high lateral resolution of FINCH.

5. Summary and conclusion

In this study, FINCH has been implemented as CAI by recording I_{PSH} in addition to a single I_{OH} and reconstructed using LR^{2}A instead of three camera shots and numerical back propagation as in conventional FINCH. Further, TAP-GSA has been used to improve the efficiency of the FINCH system. This approach of FINCH as CAI using LR^{2}A and TAP-GSA enhances the imaging characteristics of FINCH in axial resolution, SNR and efficiency while preserving its inherent high lateral resolution. In this study, an inherent problem of CAI in recording I_{PSH} was also addressed by a PSF engineering approach where by using a recorded I_{PSH} and recorded direct image of the pinhole, the ideal I_{PSH} has been synthesized. This approach prevents the loss of resolution due to I_{PSH} recorded using a larger pinhole. The preliminary results are promising for extending the developed concepts for implementing FINCH to fluorescence microscopy. In

this study, comparison study is carried out only with conventional FINCH. There are many advanced versions of FINCH that improve the temporal resolution where the performance is similar to classical FINCH and, so comparison in such cases was not needed [9, 10, 14]. Other advanced methods of FINCH, requires additional passive or active optical elements such as metalenses, liquid crystal devices including additional SLMs, and advanced sensors such as polarization cameras, and therefore the comparison in those cases will be carried out in the future [11, 13, 17–20, 22]. There are other conditions for which the method needs to be tested. In simulation, there was no constraint on the field of view as seen in the simulation results. However, in experiments, the field of view has an influence on the SNR. Further studies are needed to understand the performance of FINCH as CAI for different imaging conditions.

Data availability statement

The data that support the findings of this study are available upon reasonable request from the authors.

Acknowledgments

We thank Etienne Brasselet, CNRS, University of Bordeaux, France, for his support regarding the optical experiments.

Conflict of interest

The authors declare no conflict of interests.

Funding

This research was funded by European Union's Horizon 2020 research and innovation programme Grant Agreement No. 857627 (CIPHR) and DP240103231 from the Australian Research Council.

Author contributions

Conceptualization, V A; methodology, V A, S J, A P I X, F G A, S G, A S J F R; software, V A, S J; validation, V A, A P I X, F G A, S G, A S J F R; investigation, all the authors; resources, V A, S J; writing—original draft preparation, A P I X, F G A, V A; writing—review and editing, all the authors; supervision, V A, S J; Project administration, A S J F R; funding acquisition, V A, S J. All authors have read and agreed to the submitted version of the manuscript.

ORCID iD

Vijayakumar Anand https://orcid.org/0000-0001-8867-1949

References

[1] Rosen J and Brooker G 2007 Digital spatially incoherent Fresnel holography *Opt. Lett.* **32** 912–4
[2] Rosen J and Brooker G 2008 Non-scanning motionless fluorescence three-dimensional holographic microscopy *Nat. Photon.* **2** 190–5
[3] Katz B, Rosen J, Kelner R and Brooker G 2012 Enhanced resolution and throughput of Fresnel incoherent correlation holography (FINCH) using dual diffractive lenses on a spatial light modulator (SLM) *Opt. Express* **20** 9109–21
[4] Gustafsson M G 2000 Surpassing the lateral resolution limit by a factor of two using structured illumination microscopy *J. Microsc.* **198** 82–87
[5] Kashter Y, Vijayakumar A and Rosen J 2017 Resolving images by blurring: superresolution method with a scattering mask between the observed objects and the hologram recorder *Optica* **4** 932–9
[6] Rosen J, Vijayakumar A, Kumar M, Rai M R, Kelner R, Kashter Y, Bulbul A and Mukherjee S 2019 Recent advances in self-interference incoherent digital holography *Adv. Opt. Photonics* **11** 1–66
[7] Rosen J *et al* 2021 Roadmap on recent progress in FINCH technology *J. Imaging* **7** 197
[8] Tahara T *et al* 2022 Roadmap of incoherent digital holography *Appl. Phys.* **128** 193
[9] Nobukawa T, Muroi T, Katano Y, Kinoshita N and Ishii N 2018 Single-shot phase-shifting incoherent digital holography with multiplexed checkerboard phase gratings *Opt. Lett.* **43** 1698–701
[10] Sakamaki S, Yoneda N and Nomura T 2020 Single-shot in-line Fresnel incoherent holography using a dual-focus checkerboard lens *Appl. Opt.* **59** 6612–8
[11] Tahara T, Kanno T, Arai Y and Ozawa T 2017 Single-shot phase-shifting incoherent digital holography *J. Opt.* **19** 065705
[12] Choi K, Yim J, Yoo S and Min S-W 2017 Self-interference digital holography with a geometric-phase hologram lens *Opt. Lett.* **42** 3940–3
[13] Zhou H, Huang L, Li X, Li X, Geng G, An K, Li Z and Wang Y 2020 All-dielectric bifocal isotropic metalens for single-shot hologram generation device *Opt. Express* **28** 21549–59
[14] Tahara T, Kozawa Y, Ishii A, Wakunami K, Ichihashi Y and Oi R 2021 Two-step phase-shifting interferometry for self-interference digital holography *Opt. Lett.* **46** 669–72
[15] Anand V, Katkus T, Lundgaard S, Linklater D P, Ivanova E P, Ng S H and Juodkazis S 2020 Fresnel incoherent correlation holography with single camera shot *Opto-Electron. Adv.* **3** 200004
[16] Rai M R, Vijayakumar A and Rosen J 2018 Non-linear adaptive three-dimensional imaging with interferenceless coded aperture correlation holography (I-COACH) *Opt. Express* **26** 18143–54
[17] Kelner R, Katz B and Rosen J 2014 Optical sectioning using a digital Fresnel incoherent-holography-based confocal imaging system *Optica* **1** 70–74
[18] Bouchal P and Bouchal Z 2017 Flexible non-diffractive vortex microscope for three-dimensional depth-enhanced super-localization of dielectric, metal and fluorescent nanoparticles *J. Opt.* **19** 105606
[19] Marar A and Kner P 2021 Fundamental precision bounds for three-dimensional optical localization microscopy using self-interference digital holography *Biomed. Opt. Express* **12** 20–40
[20] Potcoava M, Mann C, Art J and Alford S 2021 Spatio-temporal performance in an incoherent holography lattice light-sheet microscope (IHLLS) *Opt. Express* **29** 23888–901

[21] Kim N, Alam M A, Bang L T, Phan A-H, Piao M-L and Erdenebat M-U 2014 Advances in the light field displays based on integral imaging and holographic techniques (Invited Paper) *Chin. Opt. Lett.* **12** 60005–9
[22] Siegel N, Lupashin V, Storrie B and Brooker G 2016 High-magnification super-resolution FINCH microscopy using birefringent crystal lens interferometers *Nat. Photon.* **10** 802–8
[23] Cieślak M J, Gamage K A A and Glover R 2016 Coded-aperture imaging systems: past, present and future development—a review *Radiat. Meas.* **92** 59–71
[24] Anand V, Katkus T, Ng S H and Juodkazis S 2021 Review of Fresnel incoherent correlation holography with linear and non-linear correlations [Invited] *Chin. Opt. Lett.* **19** 020501
[25] Gopinath S, Bleahu A, Kahro T, John Francis Rajeswary A S, Kumar R, Kukli K, Tamm A, Rosen J and Anand V 2023 Enhanced design of multiplexed coded masks for Fresnel incoherent correlation holography *Sci. Rep.* **13** 7390
[26] Vijayakumar A, Han M, Maksimovic J, Ng S H, Katkus T, Klein A, Bambery K, Tobin M J, Vongsvivut J and Juodkazis S 2022 Single-shot mid-infrared incoherent holography using Lucy-Richardson-Rosen algorithm *Opto-Electron. Sci.* **1** 210006
[27] Praveen P A, Arockiaraj F G, Gopinath S and Smith D 2022 Deep deconvolution of object information modulated by a refractive lens using Lucy-Richardson-Rosen algorithm *Photonics* **9** 625
[28] Xavier A P I, Arockiaraj F G, Gopinath S and Rajeswary A S J F 2023 Single shot 3D incoherent imaging using deterministic and random optical fields with Lucy-Richardson-Rosen algorithm *Photonics* **10** 987
[29] Bleahu A, Gopinath S, Arockiaraj F G, Rajeswary A S J F, Juodkazis S and Anand V 2023 Fresnel incoherent correlation holography with Lucy-Richardson-Rosen algorithm and modified Gerchberg-Saxton algorithm *Proc. SPIE* **125740** 125740A
[30] Vijayakumar A, Kashter Y, Kelner R and Rosen J 2016 Coded aperture correlation holography—a new type of incoherent digital holograms *Opt. Express* **24** 12430–41
[31] Bulbul A, Hai N and Rosen J 2021 Coded aperture correlation holography (COACH) with a superior lateral resolution of FINCH and axial resolution of conventional direct imaging systems *Opt. Express* **29** 42106–18
[32] Bleahu A, Gopinath S, Kahro T, Ng S H, Kukli K, Tamm A, Juodkazis S, Rosen J and Anand V 2023 Self-wavefront interference using transverse splitting holography *Results Phys.* **52** 106839